

Heat Budget of the Upper Ocean in the South-Central Equatorial Pacific

HAILONG LIU

*State Key Laboratory of Atmospheric Sciences and Geophysical Fluid Dynamics, Institute of Atmospheric Physics,
Chinese Academy of Sciences, Beijing, China*

WUYIN LIN AND MINGHUA ZHANG

Institute for Terrestrial and Planetary Atmospheres, Stony Brook University, Stony Brook, New York

(Manuscript received 12 March 2009, in final form 18 September 2009)

ABSTRACT

The double intertropical convergence zone (ITCZ) over the tropical Pacific, with a spurious band of maximum annual sea surface temperature (SST) south of the equator between 5°S and 10°S, is a chronic bias in coupled ocean–atmosphere models. This study focuses on a region of the double ITCZ in the central Pacific from 5°S to 10°S and 170°E to 150°W, where coupled models display the largest biases in precipitation, by deriving a best estimate of the mixed layer heat budget for the region. Seven global datasets of objectively analyzed surface energy fluxes and four ocean assimilation products are first compared and then evaluated against field measurements in adjacent regions. It was shown that the global datasets differ greatly in their net downward surface energy flux in this region, but they fall broadly into two categories: one with net downward heat flux of about 30 W m⁻² and the other around 10 W m⁻². Measurements from the adjacent Manus and Nauru sites of the Atmospheric Radiation Measurement Program (ARM), the Tropical Atmosphere Ocean (TAO) buoys, and the Tropical Ocean and Global Atmosphere Coupled Ocean–Atmosphere Response Experiment (TOGA COARE) are then used to show that the smaller value is more realistic. An energy balance of the mixed layer is finally presented for the region as primarily between warming from surface heat flux of 7 W m⁻² and horizontal advective cooling in the zonal direction of about 5 W m⁻², with secondary contributions from meridional and vertical advections, heat storage, and subgrid-scale mixing. The 7 W m⁻² net surface heat flux consists of warming of 210 W m⁻² from solar radiation and cooling of 53, 141, and 8 W m⁻², respectively, from longwave radiation, latent heat flux, and sensible heat flux. These values provide an observational basis to further study the initial development of excessive precipitation in coupled climate models in the central Pacific.

1. Introduction

The double intertropical convergence zone (ITCZ) in coupled ocean–atmosphere models refers to two rainfall belts symmetric to the equator in the central Pacific. In observations, a double ITCZ only appears in the boreal spring; in other seasons only one band of maximum rainfall exists to the north of the equator. In coupled ocean–atmosphere models, however, the southern maximum tends to appear throughout the year (Mechoso et al. 1995). Associated with this spurious double ITCZ are the symmetric distributions to the equator of sea surface temperature (SST), zonal currents, upwelling,

and thermocline (e.g., Zhang et al. 2007). After it was identified as a systematic bias in climate models, many studies have tried to eliminate it, since it has serious consequences on the ability of a model to realistically simulate tropical mean climate, El Niño events, and teleconnection patterns (Manganello and Huang 2009). The problem, however, is still pervasive, as has been shown to exist in almost all climate models participating in the most recent Intergovernmental Panel on Climate Change (IPCC) Fourth Assessment Report (AR4) models (Lin 2007).

While the causes of the double ITCZ may be attributed to systematic biases in component models and key feedback processes involving SST (e.g., Lin 2007; Song and Zhang 2009), it has two distinct regions that appear to have different controlling processes. One is over in eastern Pacific with maximum warm bias of SST. It is

Corresponding author address: Hailong Liu, No. 40, Hua Yan Li, Beijing 100029, China.
E-mail: lhl@lasg.iap.ac.cn

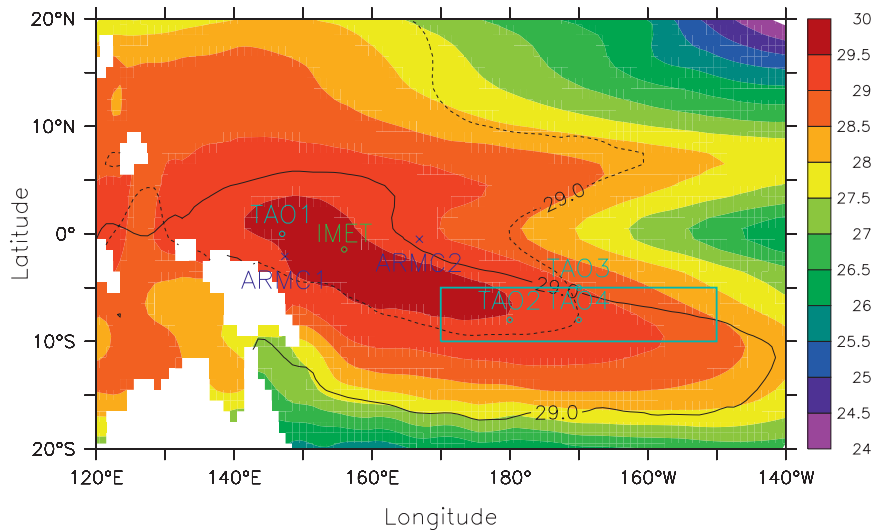


FIG. 1. The annual mean sea surface temperature (shaded; °C) from Reynolds et al. (2002). The black solid and dash contours are the 29°C isotherms for March and September, respectively. The locations of the two ARM sites (2.0°S, 147.4°E and 0.5°S, 166.9°E; blue cross), four TAO buoys (0°, 147°E; 8°S, 180°; 5°S, 170°W; and 8°S, 170°W; cyan circle) and the IMET buoy (1.45°S, 156°E; green circle) are also shown. The cyan rectangle (10°–5°S and 170°–150°W) represents the area of the double ITCZ in the south-central Pacific Ocean.

believed that deficient amount of low stratus and stratocumulus clouds play a major role in the SST biases (Ma et al. 1996; Yu and Mechoso 1999; Dai et al. 2003). The other is in the central Pacific where a distinct maximum of deep convection and precipitation appears in the models south of the equator. This spurious maximum of convection develops quickly in coupled models (H. L. Liu et al. 2009, unpublished manuscript) and it locks the surface winds, SST, and ocean currents into a biased pattern through the wind–convection feedback. In this study, we focus on this region of the double ITCZ, from 5°S to 10°S and 170°E to 150°W, which is denoted by the rectangular box in Fig. 1. Although this is not the region that SST suffers the largest error in coupled models, it is where the anomalous deep convection occurs.

The purpose of the present study is to derive the heat budget of the upper ocean over the double ITCZ where the spurious maximum convection occurs to serve as an observational constraint on the coupled ocean–atmosphere models. The diagnosis of the heat budget of the mixed layer, particularly during the early stage of the double ITCZ development, is an important step toward understanding the causes of the excessive warming and convection in the central South Pacific.

Among the heat budget terms, the net energy flux at the surface has been given in several analyzed datasets. We will therefore first examine the consistencies and differences of these datasets in describing the surface

heat flux in the target region. As will be shown later, the heat fluxes in these datasets are very different. We will thus evaluate them by using available measurements from field programs. We will finally present an estimate of the heat budget of the mixed layer ocean for the study region. Several recent studies have investigated the surface radiation and heat flux in the equatorial eastern Pacific (de Szoeke et al. 2005; Cronin et al. 2006; Fairall et al. 2008) by using data from the enhanced buoys during the Eastern Pacific Investigation of Climate Processes in the Coupled Ocean–Atmosphere System (EPIC). These studies are restricted to regions east of 110°W. The present paper complements these studies by focusing on a different region of the double ITCZ where biases in precipitation and convection are the largest in coupled models.

This paper is organized as follows. Section 2 describes the data we used, including seven objectively analyzed datasets of surface fluxes and four ocean assimilation products as well as measurements from three field programs. Section 3 presents a comparison and evaluation of the different datasets. It also gives our best estimate of the heat budget of the upper ocean in the southern branch of the double ITCZ. The last section is a summary.

2. Datasets

In the last 20 years, many efforts have been attempted to produce global gridded surface flux datasets. These

datasets can be grouped into three categories. One is the objectively analyzed surface flux data based on ship or satellite measurements of *atmospheric* surface fields (da Silva et al. 1994; Josey et al. 1998; Yu et al. 2008; Berry and Kent 2009; Large and Yeager 2008). The second is the flux data from *atmospheric* reanalyses at the operational centers (Kalnay et al. 1996; Gibson et al. 1997; Uppala et al. 2005). The third is the *oceanic* reanalysis datasets (Ji et al. 1995; Behringer and Xue 2004; Carton and Giese 2008). Since surface flux data from the atmospheric reanalyses may contain large biases on regional scales, only datasets in the first and third categories are used in this study. In addition to the gridded datasets, we also employ measurements from field programs as validation datasets. These are briefly described as follows.

a. Gridded datasets from objective analyses

The globally gridded surface heat fluxes used in this study are listed in Table 1. Objectively analyzed surface flux data typically do not use ocean measurements as input, which has been shown to create inconsistencies with energy transport in the ocean. Some datasets therefore have included adjustments to the atmosphere-based surface fluxes by imposing some broad constraint of the oceanic heat transport. The last column of Table 1 indicates which dataset has used such an adjustment.

Considering the National Ocean Center Southampton (NOCS) unadjusted version 1.1 (Josey et al. 1999) and adjusted version 1.1a (Grist and Josey 2003) as well the version 2 dataset (Berry and Kent 2009) as three separate datasets, we have used a total of seven surface flux products as listed in Table 1. Among them, the three NOCS datasets, the Oberhuber dataset (Oberhuber 1988), and the University of Wisconsin—Milwaukee—Comprehensive Ocean—Atmosphere Data Set (UMW—COADS) product (da Silva et al. 1994) are all based on ship measurements of surface winds and clouds.

The objectively analyzed air–sea heat fluxes (OAFlux) version 3 (Yu et al. 2008) used surface winds from a combination of satellite and reanalyses to calculate the latent and sensible heat fluxes. The dataset does not contain independently derived radiative fluxes, but surface radiation from the International Satellite Cloud Climatology Project (ISCCP) (Zhang et al. 2004) was included in the release. The net surface heat flux referred to as OAFlux in this study is a combination of the objectively analyzed turbulent heat fluxes and the ISCCP radiative fluxes.

The Coupled Ocean–Ice Coordinated Ocean Research Experiments (CORE) version 2 (Large and Yeager 2008) used atmospheric state variables from National Centers for Environmental Prediction (NCEP) I (Kalnay

TABLE 1. Characteristics of the global gridded surface heat flux datasets. The words in parentheses in the first column stand for the name of the datasets called in this study.

Name	Data source	Spatial resolution	Temporal resolution and period	Variables	Radiative fluxes	Turbulent fluxes	References	Constrain
Oberhuber (Oberhuber)	Climatology of COADS release 1 (Wright 1988)	2° × 2°	Climatology 1950–79	Qnet, Qsw, Qlw, Qlat, Qsen	Berliand and Berliand (1952)	Large and Pond (1982)	Oberhuber (1988)	Yes
UWM–COADS (COADS)	COADS release 1 (Woodruff et al. 1987)	1° × 1°	Monthly 1948–93	Qnet, Qsw, Qlw, Qlat, Qsen	Reed (1977); Rosati and Miyakoda (1988)	Large and Pond (1982)	da Silva et al. (1994)	Yes
NOCS v1.1 (NOCS1)	COADS release 1a voluntary observing ship (VOS) (Woodruff et al. 1993)	1° × 1°	Monthly 1980–2005	Qnet, Qsw, Qlw, Qlat, Qsen	Reed (1977); Clark et al. (1974)	Smith (1988)	Josey et al. (1999)	No
NOCS v1.1a (NOCS1a)	COADS release 1a VOS (Woodruff et al. 1993)	1° × 1°	Climatology 1980–93	Qnet, Qsw, Qlw, Qlat, Qsen	Reed (1977); Clark et al. (1974)	Smith (1988)	Grist and Josey (2003)	Yes
NOCS v2 (NOCS2)	ICOADS v2.4 VOS (Woodruff et al. 1998; Worley et al. 2005)	1° × 1°	Monthly 1973–2006	Qnet, Qsw, Qlw, Qlat, Qsen	Reed (1977); Clark et al. (1974)	Smith (1988)	Berry and Kent (2009)	No
OAFlux v3.0 (OAFlux)	Satellite and atmospheric reanalyses	1° × 1°	Monthly 1958–2006	Qlat, Qsen	—	Fairall et al. (2003)	Yu et al. (2008)	No
CORE v2 (COARE)	NCEP I, Hadley optimum interpolation (OI) SST, QuikSCAT, ISCCP Flux Data (FD)	1° × 1°	Monthly 1949–2006	Qnet, Qsw, Qlw, Qlat, Qsen	Zhang et al. (2004)	Large and Yeager (2004)	Large and Yeager (2008)	Yes

et al. 1996), and satellite scatterometer surface wind vectors from Quick Scatterometer (QuikSCAT) based on Chin et al. (1998), in the calculation of the surface turbulence heat fluxes. In addition, it adjusted the ISCCP surface insolation by a uniform reduction of 5% from 50°S to 30°N to make the zonally averaged surface flux more consistent with estimation of ocean heat transport.

Besides difference in the data sources, the datasets also differ in spatial and temporal resolutions; they cover different periods of time; they use different formulas to calculate the surface turbulent fluxes; some of them contain surface radiation while others do not. These are all listed in Table 1, along with the relevant references. The NOCS v1.1a, the Oberhuber, and the UWM-COADS, and the CORE datasets have used gross ocean transport as constraints. Given these differences, a range of heat fluxes on regional scales can be expected in the datasets, especially over the ocean where in situ measurements are sparse. We will therefore focus on the climatological annually averaged heat budget to reduce the impact of sampling errors.

b. Ocean reanalysis products

The ocean reanalysis datasets are syntheses of observations from data assimilation with numerical models. The assimilation product not only gives a dynamical description of the ocean state but also a net surface heat flux as an outcome of the thermodynamic balance of the surface layer. Because oceanic observations are used, the net surface flux is equivalent to the objective analysis with adjustment in terms of constraint by oceanic heat transport.

Four ocean reanalysis products are employed in this study to compute both the net surface heat flux and the advection terms in the heat budget equation in the targeted domain. These datasets include Simple Ocean Data Assimilation (SODA) version 2 (Carton and Giese 2008), Ocean Data Assimilation System (ODAS) RA6 (Ji et al. 1995), the new Global Ocean Data Assimilation System (GODAS) (Behringer and Xue 2004), and the Estimating the Circulation and Climate of the Ocean-Global Ocean Data Assimilation Experiment (ECCO-GODAE) at the Massachusetts Institute of Technology (MIT) version 2 (<http://www.ecco-group.org/>) (Wunsch and Heimbach 2007). Because the ocean reanalysis products do not contain the components of the surface heat flux, they can be only used to evaluate the net surface heat flux.

The bulk of ocean input data are essentially the same, but the products differ in the assimilation methods and numerical models used. SODA and GODAS have a higher horizontal resolution ($0.5^\circ \times 0.5^\circ$) and a longer

duration, from 1958 and from 1980 to the present, respectively, than the other two datasets, which both started in 1992.

c. Field program data

To evaluate the surface heat fluxes over the western equatorial warm pool from the various products described above, we have used field measurements at locations adjacent to the targeted domain. These include the two Atmospheric Radiation Measurement Program's Tropical Western Pacific (ARM TWP) sites, one on Los Negros Island in Manus (2.0°S, 147.4°E) established in 1996, the other on Nauru Island (0.5°S, 166.9°E) established in 1998. They are referred to later as ARMC1 and ARMC2, respectively (Fig. 1). The ARM sites contain surface upward and downward measurements of shortwave and longwave radiative fluxes. Because we seek to validate the gridded surface flux data over the oceans, we only used the downward shortwave radiation from the radiometers to minimize the impact of Island. The 1-min surface insolation data are first quality controlled and then averaged to monthly means; they are used to obtain the net shortwave radiative heat flux by assuming a surface albedo of 5.5% that is typical over ocean at the equator (Weller and Anderson 1996; Jin et al. 2004). The ARM data do not have surface turbulent heat fluxes.

We also used data from four Tropical Atmosphere Ocean (TAO) buoys (McPhaden et al. 1998). The buoy located at (0°, 147°E), referred to as TAO1, is collocated with the ARMC1 site at (2°S, 147°E) to cross check the ARM measurements. The other three buoys referred to as TAO2 (8°S, 180°), TAO3 (5°S, 170°W), and TAO4 (8°S, 170°W) located just in the target domain are employed to evaluate the latent heat flux from the gridded objective analysis datasets. The daily averaged net shortwave radiation and latent heat flux from the TAO buoys is directly downloaded from <http://www.pmel.noaa.gov/tao/oceansites/flux/main.html>.

Additionally, we also used the Woods Hole Oceanographic Institution Improved Meteorological Instrument (WHOI IMET) surface mooring deployed in the center of the Intensive Flux Array (IFA) at (1.45°S, 156°E) during the Tropical Ocean and Global Atmosphere Coupled Ocean-Atmosphere Response Experiment (TOGA COARE) Intensive Observation Period (IOP) (1 November 1992–28 February 1993) (Weller and Anderson 1996). The IMET data contain incoming shortwave radiation, incoming longwave radiation, and the surface meteorological and oceanic state variables. The net shortwave radiation is calculated using the same procedure as for the ARM data. The net longwave radiation is the difference between the observed downwelling

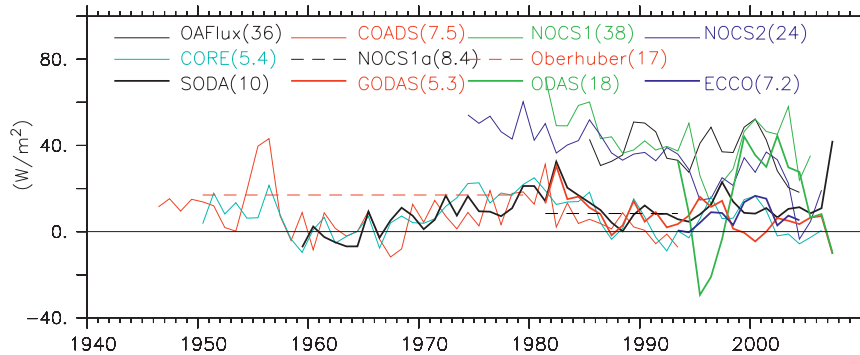


FIG. 2. The annual mean net surface heat fluxes (W m^{-2}) for seven gridded datasets (thin and dash lines) and four ocean reanalysis datasets (thick lines) averaged in the south-central Pacific Ocean shown in Fig. 1. The numbers in parenthesis are the mean values between 1993 and 2004, except those of COADS, NOCS1a, and Oberhuber, which are averaged during their own period. COADS is between 1948 and 1993, NOCS1a between 1980 and 1993, and Oberhuber between 1950 and 1979.

radiation and the outgoing longwave radiation estimated from SST. The turbulent heat fluxes are from the TOGA COARE Bulk Flux Code version 2.5b (Fairall et al. 1996). More detailed description of the datasets can be found in (Weller and Anderson 1996).

The ARM and IMET data will be used to compare with either the radiative fluxes or the total surface heat fluxes in the gridded objective or assimilation products at the same locations. Since these locations are the closest to our study domain with field program data, we consider the gridded products that agree better with the in situ data at these sites to also better describe the heat fluxes over the study domain.

3. Results

a. Net surface heat fluxes in the gridded datasets

Figure 2 shows the annual mean net surface heat fluxes, averaged from 5°S to 10°S and 170°E to 150°W , by using the seven objectively analyzed gridded datasets and the four ocean reanalysis datasets. The longest data record is from CORE, followed by UWM-COADS, and then by SODA. Most other datasets start around 1980. Two of the datasets, the Oberhuber and NOCS1a, are climatology for different nonoverlapping periods (dashed lines).

While there are interannual and decadal variabilities, the differences among different datasets are overall more significant. When averaged over time by taking the common period from 1993 to 2004, the surface net fluxes, whose values are given within the parenthesis in the legend of Fig. 2, can be divided into two groups: one with high value at around 30 W m^{-2} and the other with low value of slightly less than 10 W m^{-2} . The high-value datasets include the three unadjusted gridded datasets

of NOCS1, NOCS2, and OAFIux that has been combined with the ISCCP radiation data. Among them, NOCS1 has the largest value of 38 W m^{-2} , and the NOCS2 has the smallest value of 24 W m^{-2} . The low-value datasets include the four adjusted gridded objective analyses (UWM-COADS, NOCS1a, Oberhuber, and CORE) and the four ocean reanalysis products. Net surface fluxes in these datasets are below 10 W m^{-2} except for the Oberhuber and the ODAS: the former was climatology for an earlier period of time while the latter exhibited very large interannual variabilities. The two groups of the 11 datasets therefore show an approximate 20 W m^{-2} difference in the net surface heat fluxes in the study domain.

Other noteworthy features include the interannual and decadal variabilities in the datasets. The net surface flux in the high-value group has a decreasing trend from 1980 to 2000. The averaged values in the OAFIux, NOCS1, and NOCS2 datasets during 1984–93 are 40, 44, and 39 W m^{-2} , respectively, which should be compared with their values of 36, 38, and 24 W m^{-2} during 1993–2004. The trend is less pronounced in the low-value data group, especially after the mid-1980s. As a result, the difference of the net surface heat flux between the two groups varies with time, becoming smaller toward the end. Nevertheless, the difference is still significant and larger than the interannual variabilities, including those associated with El Niño events.

Over a period of five decades since 1955, there appears a distinctive period of maximum net downward heat flux in the early 1980s. The time coincides with the beginning of the satellite measurements and the start of the low-value group datasets. The SST in the equatorial tropical Pacific switched from the La Niña-dominated decades before 1977 to a more active El Niño period

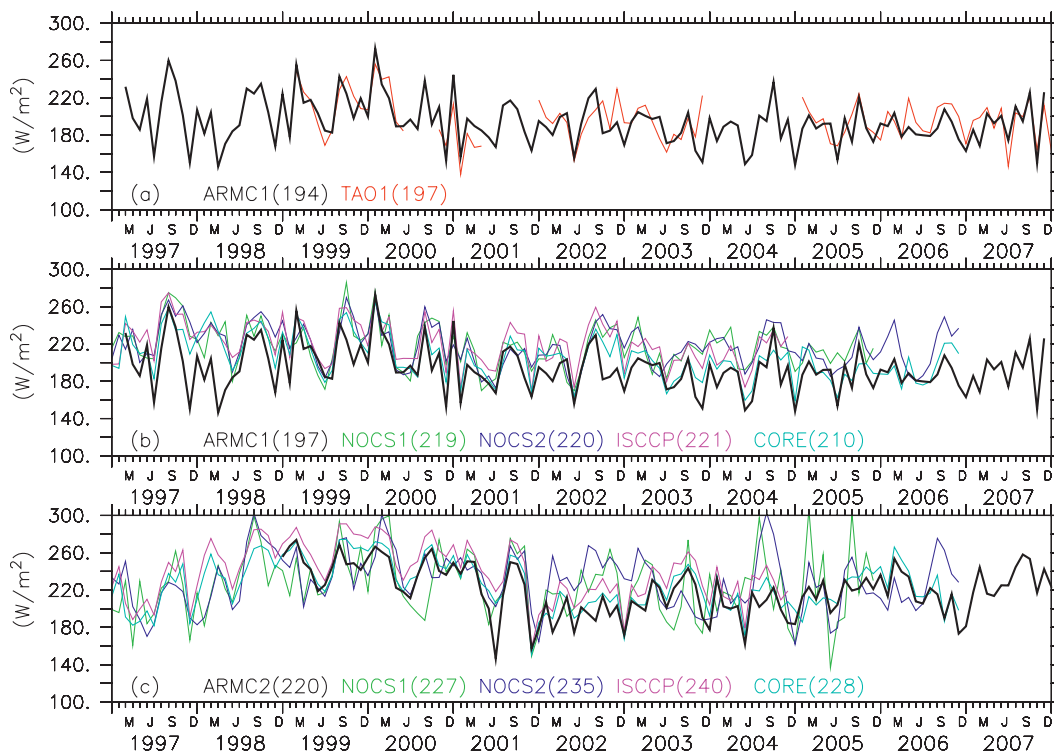


FIG. 3. (a) The monthly mean net surface shortwave radiations (W m^{-2}) for ARM C1 site (black) and nearby buoy TAO1 (red). The monthly mean net surface shortwave radiations for (b) the ARM C1 site and (c) the ARM C2 site (black) compared with other four climatic datasets (NOCS1, NOCS2, ISCCP, and CORE) at ARM's locations. The numbers in parentheses in (a) are the mean time when TAO1 buoy has observations. The numbers in (b) and (c) show the mean time over 1997–2004 and 1999–2004, respectively.

after that. The timing is consistent with the increasing trend of net surface heat flux before 1983, in which a large El Niño event occurred. It would, however, be a stretch to make more inferences from the figure because of the sparse input data, except that the magnitude of the interannual variability in the ODAS is an outlier. Given the short coverage of the ODAS data and this large interannual variability, the mean net heat flux from the ODAS will not be used.

Berry and Kent (2009) also reported a decreasing trend of the surface net heat flux in the NOCS2 datasets over the global oceans. They found that in the well-sampled area the trend is much reduced. This suggests that the trend could be also caused by changes in the sampling of input data.

Figure 2 shows the tight clustering of the three ocean assimilation products from SODA, GODAS, and ECCO and the objective analyses of NOCS1a and CORE. The UWM-COADS overlapped with these datasets before 1993, during which its flux is also very close to the others.

It therefore appears that the datasets that have used oceanic measurements either in the assimilation process or as broad constraint give a mean net downward heat

flux in the tight range of $5.3\text{--}10 \text{ W m}^{-2}$ for the double ITCZ domain after 1980. Datasets that have used atmospheric analysis of surface fluxes alone give larger net downward surface flux in the range of $24\text{--}38 \text{ W m}^{-2}$. It is not surprising that the latter category has a larger range since the net heat flux is from summing up the four separate components of surface latent and sensible heat fluxes as well as longwave and shortwave radiative fluxes. The leading terms among them are the surface latent heat flux and the downward shortwave radiation. The former is calculated by using surface winds, which have large uncertainties, and atmospheric humidity along with bulk formulas; the latter is calculated either based on eye observation of sky cloudiness and highly empirical formulas or from ISCCP. In the following, we evaluate the shortwave radiation component of the total heat budget by using available field program data.

b. Comparison of shortwave radiation with ARM and TAO measurements

Figure 3a shows the monthly mean surface net downward shortwave radiation at ARM C1 and the nearby TAO buoy (TAO1). Regardless of the anticipated variability

in clouds and thus radiation, the data from ARMC1 are quite steady throughout the 11-year period. Results from TAO1 track the ARM value remarkably well, even in the month-to-month variations. When averaged over the time period with available data, the net shortwave radiation at ARMC1 is 194 W m^{-2} ; it is 197 W m^{-2} at TAO1. This consistency lends some confidence on the field program data.

The monthly mean net surface shortwave fluxes at the ARMC1 site from the NOCS1, NOCS2, ISCCP, and CORE are shown in Fig. 3b, along with values from the ARM measurements. As mentioned before, the CORE radiative flux is a uniform reduction of 5% of the ISCCP value, while the two versions of the NOCS data are based on visual estimates of total cloud cover made by the reporting officer on ships in the units of tenths and empirical formulas that were calibrated against limited amount of in situ measurements at other locations. The two NOCS data are close to each other and to the ISCCP values. While they reasonably track the main features of the interannual variability in the ARM data, there is a systematic difference in the mean values of the surface radiation. Over the period of 1997–2004, they are 219, 220, and 221 W m^{-2} for NOCS1, NOCS2, and ISCCP, respectively. These are about 10% or 20 W m^{-2} larger than the ARM data. The value in the CORE, with the 5% reduction of the ISCCP data, is therefore still about 10 W m^{-2} larger than the ARM data. A decrease of the ocean surface albedo from 5.5% to 5.0%, which is at the low end of available albedo estimates (Jin et al. 2004), in the calculation of the ARM net shortwave flux would increase the ARM value by only 1 W m^{-2} . This change is too small to explain the differences.

The net surface shortwave radiations from ARM at the ARMC2 are shown in Fig. 3c (black line). The interannual variability is larger at this location. In particular, the four La Niña periods during 1999–2001, in 2003, in 2005, and in 2007–08, can be clearly identified with larger values of net downward surface radiation. As shown in Fig. 1, in which the 29°C SST contours for March (solid) and September (dashed) are over plotted on the annual mean SST, the ARMC2 site is near the boundary of the warm pool. It is therefore subject to a larger impact of the ENSO events. The larger magnitude of the downward shortwave radiation at ARMC2 than that at ARMC1 is because of the overall decrease of clouds away from the warm pool.

Figure 3c further shows the comparisons of ARMC2 measurements with the gridded analyses. The ISCCP value of 240 W m^{-2} is also about 20 W m^{-2} larger than the ARM data. The CORE is thus about 10 W m^{-2} larger. The NOCS1 and NOCS2 values are 227 W m^{-2} and 235 W m^{-2} , respectively, during the ARMC2 record

from 1999 to 2004. The location of ARMC2 being near the boundary of the warm pool makes it less ideal to cross evaluate the data, but the overall larger shortwave radiation than the field program data can be seen at this site.

The above discussions suggest an overestimation of surface shortwave radiation in the unconstrained datasets by about 20 W m^{-2} in the broad warm pool region, and this value is sufficiently large to explain the differences in the net downward surface heat fluxes in the two groups of data in Fig. 2. The CORE data, having similar net heat flux to those in other constrained datasets but with larger radiation flux by about 10 W m^{-2} , likely have compensation from overestimated surface turbulent heat fluxes.

Oberhuber (1988) reported that, after decreasing the insolation in COADS by 10%, a reasonable implied ocean meridional heat transport can be obtained. Comparing with TAO buoys, Taylor et al. (1999) also found a 24 W m^{-2} overestimation in downward shortwave heating in the NOCS1 dataset over the warm pool. Using a linear inverse analysis and the 10 hydrographic ocean heat transport constraints distribution, Grist and Josey (2003) got a fairly good estimation of surface heat flux in the warm pool when an adjustment of the shortwave radiation between 6% and 9% are made. These results are consistent with the present analysis.

c. Comparison of latent heat flux with TAO measurements

To confirm the results present above, we further evaluate another leading term of the four components of net surface flux and latent heat flux in the target domain by using the TAO buoy data. Figure 4 shows the monthly mean latent heat flux average at three TAO buoy sites in the study domain from TAO buoys, NOCS1, NOCS2, OAFlux, and CORE. When averaged over the time period with available data, the latent heat flux at TAO buoys is -135 W m^{-2} ; the values for NOCS1 and OAFlux are both -138 W m^{-2} . This consistency further confirms that it is the overestimated shortwave radiations lead these two datasets fall into the high-value group. Taylor et al. (1999) and Yu et al. (2008) have also compared NOCS1 and OAFlux with TAO buoys. Their results are consistent with the present study.

The latent heat fluxes are overestimated in the CORE dataset by about 10 W m^{-2} . This value just offsets the overestimated shortwave radiations in this dataset. It explains that why the CORE data have similar net heat flux to those in other constrained datasets but with larger radiation flux by about 10 W m^{-2} . For the NOCS2 dataset, latent heat flux is overestimated by about 20 W m^{-2} . This by itself would offset the overestimated shortwave

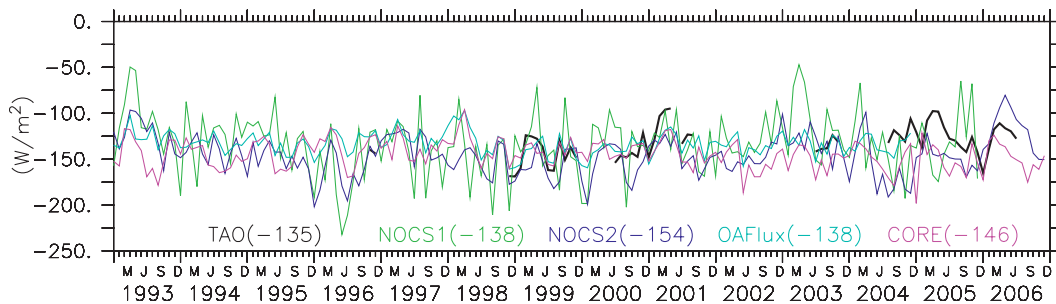


FIG. 4. The monthly mean latent heat flux (W m^{-2}) averaged at the three TAO buoy sites in the target domain for TAO buoys (black), NOCS1 (green), NOCS2 (blue), OAFflux (cyan), and CORE (purple). The numbers in parentheses are the time mean when TAO buoys has observations.

radiation shown earlier. A further examination shows that there is an additional bias in the upward longwave radiation in NOCS2 that is underestimated by about $10\text{--}15 \text{ W m}^{-2}$. This is because the longwave flux formula has a tendency to underestimate the upward flux (Taylor 2000).

Therefore, among the gridded datasets that overestimate the net surface fluxes, shortwave radiation is universally overestimated by about 20 W m^{-2} . Latent heat fluxes are reasonable in the NOCS1 and OAFflux datasets but overestimated in the NOCS2 and CORE datasets, with the latter two containing additional compensating errors. These features can be further confirmed in the comparison with measurements from TOGA COARE.

d. Comparison with IMET data

We compare the gridded datasets to the WHOI IMET buoy deployed at 1.45°S , 156°E during the TOGA COARE IOP. Figure 5a shows the differences of the net downward shortwave radiation in the four gridded datasets of OAFflux (ISCCP), NOCS1, NOCS2, and CORE with the IMET data. Consistent with the ARM TWP and TAO buoy comparison, all these datasets overestimated surface shortwave radiation by about 20 W m^{-2} , except for CORE in which the difference is 6 W m^{-2} . The TOGA CORE IMET data also indicated underestimation of net upward longwave radiation flux by about 10 W m^{-2} in all the four gridded datasets (not shown). The IMET net upward longwave radiation of 58 W m^{-2} , however, is calibrated against the downwelling longwave Rapid Radiative Transfer Model (RRTM) for clear-sky conditions, but an independent radiative transfer calculation by Curry et al. (2004) suggested net longwave flux of 45 W m^{-2} , while measurements based on research vessel (R/V) *Moana Wave* showed 53 W m^{-2} (Curry et al. 2004). It is therefore difficult to conclude whether there is a systematic bias of the longwave radiation in the gridded objective analysis at the buoy location.

Figure 5b shows the difference of the latent heat flux in the four gridded datasets with the IMET buoy data. Negative value corresponds to less energy to the ocean and more to the atmosphere. Relative to IMET, all gridded datasets overestimated the latent heat flux to various degrees. Curry et al. (2004), however, computed a latent heat flux of 120 W m^{-2} rather than the IMET value of 108 W m^{-2} —a difference of 12 W m^{-2} when they used the same flux algorithm of Fairall et al. (1996) but with winds for a $0.5^{\circ} \times 0.5^{\circ}$ grid box. If the Curry et al. (2004) value is used, only the NOCS2 and CORE latent heat fluxes are overestimated, with the CORE by as much as about 40 W m^{-2} . This is consistent with the comparison we have done in the previous subsection.

The differences of net downward heat flux between the four gridded datasets and the IMET data are shown in Fig. 5c. The net downward heat flux is overestimated in OAFflux and NOCS1, with a magnitude of about $10\text{--}20 \text{ W m}^{-2}$ that is comparable to the shortwave bias. The overestimation is smaller in NOCS2, but this is the result of offsetting the shortwave bias by the overestimation of latent heat flux. The downward net heat flux in CORE is about 40 W m^{-2} smaller than the IMET value because of the very large surface latent heat flux.

Because TOGA COARE only covers the four months of November 1992 to February 1993, the above comparison is subject to large impact from differences in temporal and spatial samplings. Nevertheless, some systematic biases still emerge: there is an overall overestimation of about 20 W m^{-2} in net downward surface shortwave radiation in the unconstrained objectively analyzed surface flux data, which can largely explain the difference of similar magnitude in the net surface heat flux.

e. The heat budget in the region of double ITCZ

The above discussions lead us to conclude that among the two groups of net surface flux data in Fig. 2, the low-value group is more reliable than the high-value group

TABLE 2. The mixed layer heat budget (W m^{-2}) over the south-central equatorial Pacific ($10^{\circ}\text{--}5^{\circ}\text{S}$, $170^{\circ}\text{E}\text{--}150^{\circ}\text{W}$) for four ocean reanalysis datasets during 1993–2004. The mixed layer depths and temperatures are also shown.

	SODA	ODAS	GODAS	ECCO
Mixed layer depth (m)	81	83	87	70
Temperature tendency ($^{\circ}\text{C}$)	0.6	0.5	0.6	0.2
Surface flux	10.2	18.2	5.2	7.2
Horizontal advection [(east–west)/(north–south)]	–6.7 (–8.4/1.7)	–6.5 (–9.4/2.9)	–6.0 (–8.3/2.3)	–6.3 (–8.0/1.7)
Residual (vertical advection)	–2.9 (1.4)	–11.2	1.4	–0.7 (1.5)

in describing the net surface heat flux in the tropical Pacific. This group includes UWM–COADS, NOCS1a, CORE, and the three ocean reanalyses of SODA, GODAS, and ECCO.

We therefore proceed to calculate the transport of heat for our study domain by using the ocean currents and temperature in the reanalysis data. The thermodynamic equation of the ocean, when vertically integrated, is written as follows:

$$\rho_0 C_p h \frac{\partial \langle T \rangle}{\partial t} = -\rho_0 C_p h \left\langle \frac{\partial u T}{\partial x} + \frac{\partial v T}{\partial y} \right\rangle + Q_0 + R,$$

where the bracket represents vertical average over the mixed layer; h is the mixed layer depth; Q_0 is the net downward surface heat flux; and R is the sum of vertical advection and all subgrid-scale processes such as horizontal diffusion, the vertical diffusion at the bottom of the mixed layer, and convective process. This term includes entrainment of cold water into the mixed layer from below. Here ρ_0 [$1026 \text{ kg (m}^{-3}\text{)}$] is the reference oceanic density, and C_p [$3996 \text{ J (kg K)}^{-1}$] denotes the specific heat of seawater.

We use monthly averaged data to compute the heat budget. Calculation with daily data shows little differences for the results presented below. The mixed layer is defined in the present study as the depth of isotherm that is 0.5°C colder than the SST. Here, the method of Lee et al. (2004) is used to compute the temperature advection term. Their formulation is expressed as advection of interface temperature referenced to the spatially averaged temperature of the study domain. So it is suitable to evaluate effects of external processes on the domain-averaged temperature. The volume-averaged temperature of the target domain is used as the reference temperature.

Table 2 shows the long-term averages of the heat budget of the ocean mixed layer and its depth from the three oceanic reanalyses in the double ITCZ region. The surface heating is primarily balanced by the cooling of similar magnitude from the horizontal advection. The cold advection in the zonal direction dominates the total advection. Advection in the meridional direction is an

effect of warming, but with a smaller magnitude. The other terms—including the vertical advection, the heat storage, and the subgrid-scale transport—are smaller. Only SODA and ECCO provide vertical velocities. While the calculation of the heat transport itself contains uncertainties, the consistency among the datasets gives some confidence about the magnitude.

The prevailing wind in this region is a southeast trade wind. In the zonal direction, the easterly drives a westward surface current, the South Equatorial Current (SEC) (Fig. 6, zonal current in the three reanalyses). Since the water temperature of this region is higher than that to its east, the SEC transports cold water to cool the double ITCZ region. Stevenson and Niiler (1983) studied the heat budget by using measurements from the Hawaii-to-Tahiti Shuttle Experiment (February 1979–June 1980) for a region to the east of our study domain. They found that the advection of cold water from the east is important in explaining the seasonal evolution of SST. This is consistent with our results. In the meridional direction, the surface poleward Ekman currents are mainly in the upper 50 m, while the flows below 50 m are equatorward (Fig. 7). The small positive advection of temperature in the meridional direction is hence a result of the equatorward ocean flow beneath the surface southward current that is associated with equatorial upwelling (Fig. 6).

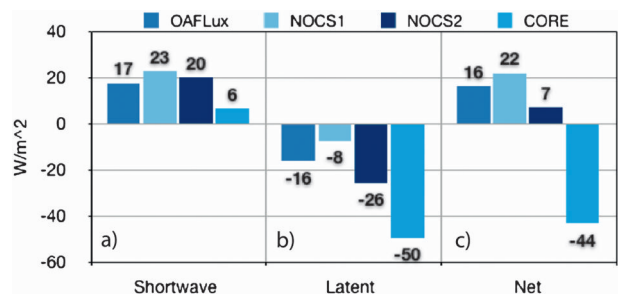


FIG. 5. The differences of (a) the net shortwave radiation, (b) the latent heat flux, and (c) the net surface heat flux between four climatic datasets (OAFLux, NOCS1, NOCS2, and CORE) and IMET buoy averaged during TOGA COARE IOP (Nov 1992–Feb 1993). Downward is positive.

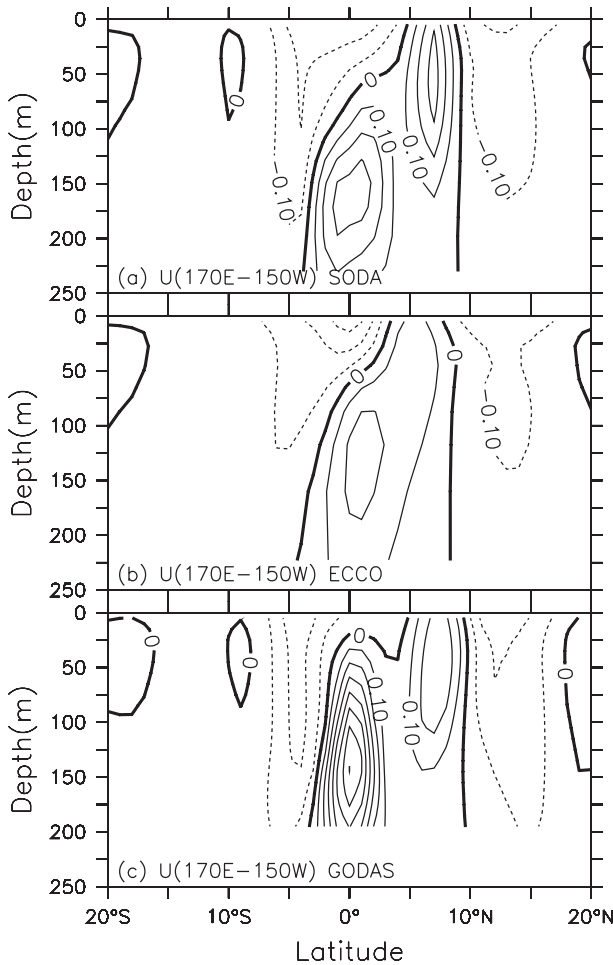


FIG. 6. The zonal currents (m s^{-1}) averaged over 170°E – 150°W for (a) SODA, (b) ECCO, and (c) GODAS.

There are some differences in the depth of the mixed layer in Table 2 as defined in this study, with the temperature in ECCO more vertically stratified in the region of double ITCZ. We therefore also calculated the heat budget for the top 50 m of the upper ocean, which is shallower than the layer used in Table 2. The budget terms are shown in Table 3. As expected, the magnitude of the horizontal advection is reduced correspondingly, especially in the meridional direction; the southward current due to the equatorial upwelling plays a larger role. The reduced horizontal cooling is made up by the cooling from the residual term, likely because of vertical mixing at the bottom of the layer.

A schematic summary of the heat budget for the upper ocean of 50 m is given in Fig. 8. We have used the mean net surface heat flux from the six datasets of the low-value group in Fig. 1: UWM-COADS, NOCS1a, CORE, SODA, GODAS, and ECCO. It would be more satisfying if an error uncertainty can be attached, but the

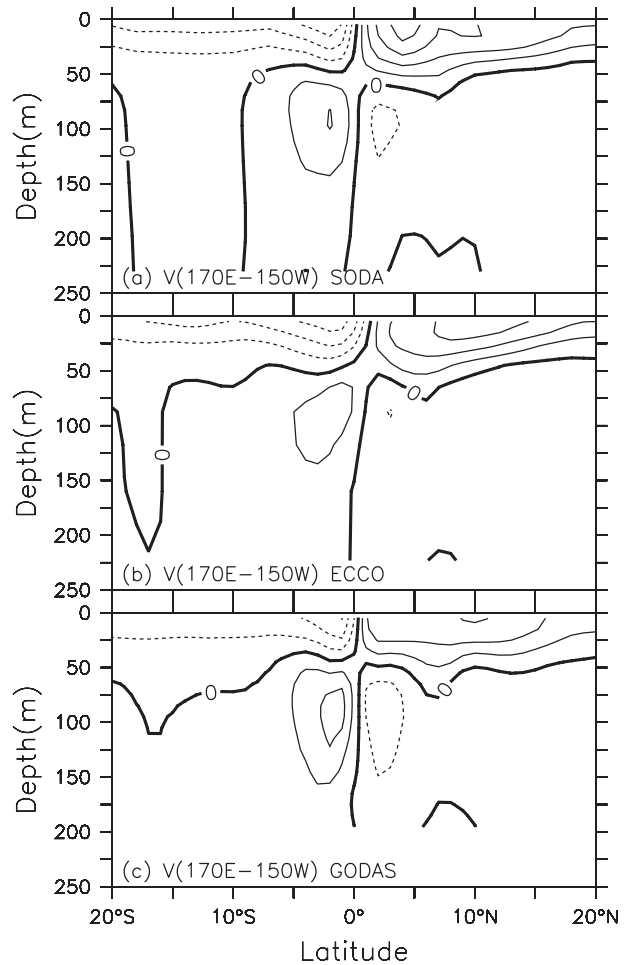


FIG. 7. Same as Fig. 6, but for the meridional currents (m s^{-1}). The contour interval is 0.02.

complex approaches that have been used in the construction of each dataset prevented us from giving a credible estimate. Instead, we have included the range of the values from the different datasets in the parenthesis. On average, the region receives 7 W m^{-2} of energy from the surface; it exports 5 W m^{-2} of heat because of the cold advection in the zonal direction and 2 W m^{-2} because of the subgrid-scale mixing at the bottom of the layer. The warming from the meridional advection is about the same as the heat storage term at about 0.2 W m^{-2} , which corresponds to an approximate warming of about $0.03^{\circ}\text{C yr}^{-1}$.

These heat fluxes are one to two orders of magnitude smaller than the individual heat components at the surface of shortwave, longwave, latent, and sensible heat fluxes. We give an estimate of these components in Fig. 7, which are not available in the ocean assimilation products. It is based on NOCS1a data because it agrees with the best estimate of the net surface flux, and its

TABLE 3. The upper-50-m heat budget (W m^{-2}) over the south-central equatorial Pacific ($10^{\circ}\text{--}5^{\circ}\text{S}$, $170^{\circ}\text{E}\text{--}150^{\circ}\text{W}$) for four ocean reanalysis datasets during 1993–2004.

	SODA	ODAS	GODAS	ECCO
Temperature tendency ($^{\circ}\text{C}$)	0.3	0.3	0.3	0.1
Surface flux	10.2	18.2	5.2	7.2
Horizontal advection [(east–west)/(north–south)]	–5.6 (–4.9/–0.7)	–5.0 (–5.5/0.5)	–4.4 (–4.9/0.5)	–5.3 (–6.2/0.9)
Residual (vertical advection)	–4.3 (1.3)	–12.9	–0.5	–1.8 (0.7)

shortwave radiation being about 20 W m^{-2} less than the other gridded datasets is also in line with the evaluations above. Over the double ITCZ region, the time mean values of the shortwave and longwave radiation at the surface is around 209 and 53 W m^{-2} , respectively, and the sensible heat fluxes are about 141 and 8 W m^{-2} , respectively, leaving about 7 W m^{-2} of net downward heat flux to the ocean.

f. Comparison with heat budget in the counterpart in the Northern Hemisphere

In the above study, we have focused on the heat budget of the maximum SST band in the Southern Hemisphere where the largest biases in deep convection occur in coupled models. Since the double ITCZ in the coupled models is characteristic of two convective zones in both hemispheres, we also carried out the heat budget calculation for the same longitudes but between 5° and 10°N . This is a region of observed maximum SST band with observed ITCZ in precipitation. The mixed layer depths and the terms of heat budget of this region are shown in Table 4. It is seen that, unlike the region south of the equator, the net surface heat flux is close to zero. The mixed layer is maintained by large warm advectations from ocean currents and mixing as represented by the residual terms. The North Equatorial Counter Current transports warm water from west to east and warms this region. Similar to the southern region, the effect of temperature advectations in meridional direction on the mixed layer is also warming from the equatorward returning circulation, but the magnitude is larger because of the larger temperature gradient in the Northern Hemisphere than that in the Southern Hemisphere.

4. Summary and discussion

We have compared the net surface heat flux in the central Pacific south of the equator where the spurious double ITCZ occurs in coupled ocean–atmosphere models by using seven objectively analyzed gridded datasets and four ocean data assimilation products. We showed that the heat flux in the study domain can be

categorized into two different groups with annual mean values of about 10 W m^{-2} and 30 W m^{-2} , respectively. All ocean assimilation products and those objective analyses that had empirically adjusted the surface heat flux with some broad constraint of ocean heat transport are in the low-value group, while objective analyses that did not apply ocean transport constraint are in the high-value group. Heat fluxes in the second group are constructed from summing up the surface radiative and latent as well as sensible heat fluxes. We have used the ARM surface shortwave radiation at its tropical western Pacific sites, and from the collocated TAO buoy, as well as measurements from the TOGA COARE IMET buoy to show that the shortwave radiation in the unconstrained datasets are about 20 W m^{-2} larger than in situ measurements. Then, latent heat fluxes at three TAO buoys are used to show that the latent heat fluxes in most datasets agree with measurements from filed programs, except for NOCS2 and CORE. Therefore,

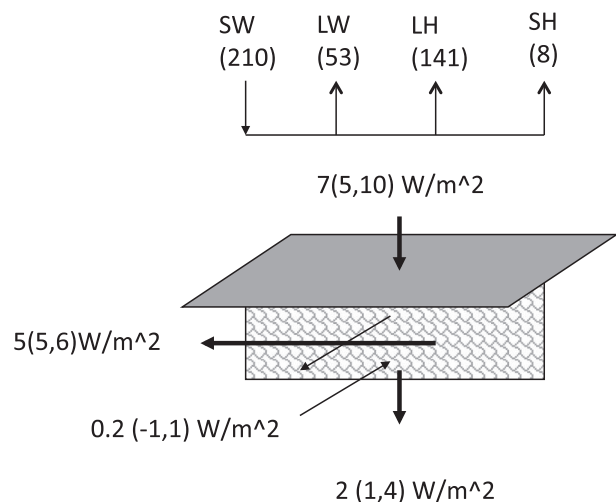


FIG. 8. The schematic figure of heat budget of upper 50 m in the south-central equatorial Pacific. The net surface flux, zonal and meridional temperature advection, and the residual terms are the mean value of three oceanic reanalysis datasets (SODA, GODAS, and ECCO). The numbers in parentheses are the ranges of these terms. Four components of the net surface heat flux are all from NOCS1a.

TABLE 4. The mixed layer heat budget (W m^{-2}) over the north-central equatorial Pacific (5° – 10°N , 170°E – 150°W) for four ocean reanalysis datasets during 1993–2004. The mixed layer depths and temperatures are also shown.

	SODA	ODAS	GODAS	ECCO
Mixed layer depth (m)	60	61	66	47
Temperature tendency ($^{\circ}\text{C}$)	0.6	0.2	0.5	0.5
Surface flux	0.7	0.2	–8.6	0.8
Horizontal advection [(east–west)/(north–south)]	24.5 (13.5/11.0)	34.0 (12.5/21.5)	20.3 (12.3/8.0)	21.8 (10.8/20.0)
Residual (vertical advection)	–24.6 (–4.7)	–34.0	–11.2	–22.1 (–4.0)

surface heat fluxes in the low-value datasets are considered more reliable than those in the high-value datasets.

We have presented the following mean heat budget for the upper 50 m of the ocean in the study domain: surface warming of about 7 W m^{-2} is balanced by heat loss of 5 W m^{-2} from zonal advection and 2 W m^{-2} and from subgrid-scale mixing at the bottom of the layer. These values, one to two orders of magnitude smaller than the surface shortwave radiation and latent heat flux, point to the difficulties in constructing reliable net surface heat flux from the large individual components.

The culprit of the inconsistency among the various flux datasets is the surface insolation. Absorption of solar radiation in the atmosphere by clouds and aerosols has been extensively studied in the past (Cess et al. 1995; Ramanathan et al. 1995). Several investigations have reported that the incoming shortwave radiation at the surface is overestimated in most numerical models and likely in various satellite algorithms (e.g., Yu et al. 1999, Large and Yeager 2008; Trenberth and Smith 2008), but a conclusive reconciliation has yet to take place. The ship-based empirical estimation of shortwave radiation, on the other hand, could be too crude to yield satisfactory net surface flux estimations.

Although knowing the heat budget of the upper ocean will not offer direct insights on how to reduce the double ITCZ biases in coupled models, it can provide an observational basis to evaluate the models, especially in spinup experiments when the model biases initially develop, in which case the causes of errors in surface flux or ocean currents may be identified. Zhang et al. (2007) described a feedback mechanism in which double ITCZ develops in coupled models when an initial heat flux bias causes spurious zonal advection of ocean temperature, which in turn feeds back to the heat flux. We intend to use the analysis presented in this study to constrain the different components of the energetics of the upper ocean in coupled models. Results from the controlled and sensitivity experiments will be reported elsewhere.

Acknowledgments. We wish to thank Dr. Carlos Mechoso and the two anonymous reviewers for their very valuable comments that have helped to improve our paper. This research is supported by the Climate Change and Prediction Program and the atmospheric Radiation Measurement Program of the U.S. Department of Energy. Additional support is provided by NASA and the U.S. National Science Foundation to Stony Brook University. This work was conducted during a visit of Hailong Liu to Stony Brook University. Hailong Liu is also supported by the National Natural Science Foundation of China under Grant 40775054 and the National Key Program for Developing Basic Sciences Grant 2007CB411800.

REFERENCES

- Behringer, D., and Y. Xue, 2004: Evaluation of the global ocean data assimilation system at NCEP: The Pacific Ocean. Preprints, *Eighth Symp. on Integrated Observing and Assimilation Systems for Atmosphere, Oceans, and Land Surface*, Seattle, WA, Amer. Meteor. Soc., 2.3. [Available online at <http://ams.confex.com/ams/pdfpapers/70720.pdf>.]
- Berliand, M. E., and T. G. Berliand, 1952: Determining the net longwave radiation of the Earth with consideration of the effect of cloudiness. *Isv. Akad. Nauk. SSSR Ser. Geofiz.*, **1**, 64–78.
- Berry, D. I., and E. C. Kent, 2009: A new air–sea interaction gridded dataset from ICOADS with uncertainty estimates. *Bull. Amer. Meteor. Soc.*, **90**, 645–656.
- Carton, J. A., and B. S. Giese, 2008: A reanalysis of ocean climate using Simple Ocean Data Assimilation (SODA). *Mon. Wea. Rev.*, **136**, 2999–3017.
- Cess, R. D., and Coauthors, 1995: Absorption of solar radiation by clouds: Observation versus models. *Science*, **267**, 496–499.
- Chin, T., R. Miliff, and W. Large, 1998: Basin-scale high-wavenumber sea surface wind fields from multiresolution analysis of scatterometer data. *J. Atmos. Oceanic Technol.*, **15**, 741–763.
- Clark, N. E., R. M. Eber, J. A. Renner, and J. F. T. Saur, 1974: Heat exchange between ocean and atmosphere in the eastern North Pacific for 1961–71. NOAA Tech. Rep. NMFS SSRF-682, 108 pp.
- Cronin, M. F., C. W. Fairall, and M. J. McPhaden, 2006: An assessment of buoy-derived and numerical weather prediction surface heat fluxes in the tropical Pacific. *J. Geophys. Res.*, **111**, C06038, doi:10.1029/2005JC003324.
- Curry, J. A., and Coauthors, 2004: SEAFLEX. *Bull. Amer. Meteor. Soc.*, **85**, 409–424.

- Dai, F., R. Yu, X. Zhang, Y. Yu, and J. Li, 2003: The impact of low-level cloud over the eastern subtropical Pacific on the “double ITCZ” in LASG FGCM-0. *Adv. Atmos. Sci.*, **20**, 461–474.
- da Silva, A., C. Young, and S. Levitus, 1994: *Algorithms and Procedures*. Vol. 1, *Atlas of Surface Marine Data 1994*, NOAA Atlas NESDIS 6, 83 pp.
- de Szoeke, S. P., C. S. Bretherton, N. A. Bond, M. F. Cronin, and B. M. Morley, 2005: EPIC 95°W observations of the eastern Pacific atmospheric boundary layer from the cold tongue to the ITCZ. *J. Atmos. Sci.*, **62**, 426–442.
- Fairall, C. W., E. F. Bradley, D. P. Rogers, J. B. Edson, and G. S. Young, 1996: Bulk parameterization of air–sea fluxes for tropical ocean–global atmosphere coupled ocean–atmosphere response experiment. *J. Geophys. Res.*, **101**, 3747–3767.
- , —, J. E. Hare, A. A. Grachev, and J. B. Edson, 2003: Bulk parameterization of air–sea fluxes: Updates and verification for the COARE algorithm. *J. Climate*, **16**, 571–590.
- , J. E. Hare, T. Uttal, D. Hazen, M. Cronin, N. A. Bond, and D. Veron, 2008: A seven-cruise sample of clouds, radiation, and surface forcing in the equatorial eastern Pacific. *J. Climate*, **21**, 655–673.
- Gibson, J. K., P. Kallberg, S. Uppala, A. Hernandez, A. Nomura, and E. Serrano, 1997: ERA description. ECMWF Reanalysis Project Rep. Series 1, European Centre for Medium Range Weather Forecasts, Reading, United Kingdom, 71 pp.
- Grist, J., and S. Josey, 2003: Inverse analysis adjustment of the SOC air–sea flux climatology using ocean heat transport constraints. *J. Climate*, **16**, 3274–3295.
- Ji, M., A. Leetmaa, and J. Derber, 1995: An ocean analysis system for seasonal to interannual climate studies. *Mon. Wea. Rev.*, **123**, 460–481.
- Jin, Z., T. Charlock, W. Smith Jr., and K. Rutledge, 2004: A parameterization of ocean surface albedo. *Geophys. Res. Lett.*, **31**, L22301, doi:10.1029/2004GL021180.
- Josey, S., E. Kent, and P. Taylor, 1998: The Southampton Oceanography Centre (SOC) ocean–atmosphere heat, momentum and freshwater flux atlas. Tech. Rep. 6, Southampton Oceanography Centre, 306 pp.
- , —, and —, 1999: New insights into the ocean heat budget closure problem from analysis of the SOC air–sea flux climatology. *J. Climate*, **12**, 2856–2880.
- Kalnay, E., and Coauthors, 1996: The NCEP/NCAR 40-Year Reanalysis Project. *Bull. Amer. Meteor. Soc.*, **77**, 437–471.
- Large, W. G., and S. Pond, 1982: Sensible and latent heat flux measurements over the ocean. *J. Phys. Oceanogr.*, **12**, 464–482.
- , and S. G. Yeager, 2004: Diurnal to decadal global forcing for ocean and sea ice models: The data sets and climatologies. Tech. Rep. TN-460+STR, NCAR, 105 pp.
- , and —, 2008: The global climatology of an interannually varying air–sea flux data set. *Climate Dyn.*, **24**, 341–364, doi:10.1007/s00382-008-0441-3.
- Lee, T., I. Fukumori, and B. Tang, 2004: Temperature advection: Internal versus external processes. *J. Phys. Oceanogr.*, **34**, 1936–1944.
- Lin, J., 2007: The double-ITCZ problem in IPCC AR4 coupled GCMs: Ocean–atmosphere feedback analysis. *J. Climate*, **20**, 4497–4525.
- Ma, C. C., C. R. Mechoso, A. W. Robertson, and A. Arakawa, 1996: Peruvian stratus clouds and the tropical Pacific circulation: A coupled ocean–atmosphere GCM study. *J. Climate*, **9**, 1635–1645.
- Manganello, J., and B. Huang, 2009: The influence of systematic errors in the southeast Pacific on ENSO variability and prediction in a coupled GCM. *Climate Dyn.*, **32**, 1015–1034.
- McPhaden, M. J., and Coauthors, 1998: The Tropical Ocean–Global Atmosphere (TOGA) observing system: A decade of progress. *J. Geophys. Res.*, **103** (C7), 14 169–14 240.
- Mechoso, C. R., and Coauthors, 1995: The seasonal cycle over the tropical Pacific in coupled ocean–atmosphere general circulation models. *Mon. Wea. Rev.*, **123**, 3825–3838.
- Oberhuber, J. M., 1988: An atlas based on COADS data set: The budgets of heat buoyancy and turbulent kinetic energy at the surface of the global ocean. Tech. Rep. 15, Max-Planck-Institut für Meteorologie, 20 pp.
- Ramanathan, V., B. Subasilar, G. J. Zhang, W. Conant, R. D. Cess, J. T. Kiehl, H. Grassl, and L. Shi, 1995: Warm pool heat budget and shortwave cloud forcing: A missing physics? *Science*, **267**, 499–502.
- Reed, R. K., 1977: On estimating insolation over the ocean. *J. Phys. Oceanogr.*, **7**, 482–485.
- Reynolds, R. W., N. A. Rayner, T. M. Smith, D. C. Stokes, and W. Wang, 2002: An improved in situ and satellite SST analysis for climate. *J. Climate*, **15**, 1609–1625.
- Rosati, A., and K. Miyakoda, 1988: A general circulation model for upper ocean simulations. *J. Phys. Oceanogr.*, **18**, 1601–1626.
- Smith, S. D., 1988: Coefficients for sea surface wind stress, heat flux, and wind profiles as a function of wind speed and temperature. *J. Geophys. Res.*, **93** (C12), 15 467–15 472.
- Song, X., and G. J. Zhang, 2009: Convection parameterization, tropical Pacific double ITCZ, and upper-ocean biases in the NCAR CCSM3. Part I: Climatology and atmospheric feedback. *J. Climate*, **22**, 4299–4315.
- Stevenson, J., and P. Niiler, 1983: Upper ocean heat budget during the Hawaii-to-Tahiti shuttle experiment. *J. Phys. Oceanogr.*, **13**, 1894–1907.
- Taylor, P. K., Ed., 2000: Intercomparison and validation of ocean–atmosphere energy flux fields. Final Rep. of the Joint WCRP/SCOR Working Group on Air–Sea Fluxes. WCRP-112, WMO/TD-1036, 306 pp.
- , S. A. Josey, and E. C. Kent, 1999: A comparison of climatological, model derived and observed air–sea flux values for the COARE area. *Proc. Conf. on the TOGA Coupled Ocean–Atmosphere Response Experiment (COARE)*, Vol. WCRP-107, WMO/TD 940, Boulder, CO, WMO, 249–250.
- Trenberth, K. E., and L. Smith, 2008: The three dimensional structure of the atmospheric energy budget: Methodology and evaluation. *Climate Dyn.*, **32**, 1065–1079, doi:10.1007/s00382-008-0389-3.
- Uppala, S. M., and Coauthors, 2005: The ERA-40 Re-Analysis. *Quart. J. Roy. Meteor. Soc.*, **131**, 2961–3012.
- Weller, R., and S. Anderson, 1996: Surface meteorology and air–sea fluxes in the western equatorial Pacific warm pool during the TOGA Coupled Ocean–Atmosphere Response Experiment. *J. Climate*, **9**, 1959–1990.
- Woodruff, S. D., R. J. Slutz, R. L. Jenne, and P. M. Steurer, 1987: A comprehensive ocean–atmosphere data set. *Bull. Amer. Meteor. Soc.*, **68**, 1239–1250.
- , S. J. Lubker, K. Wolter, S. J. Worley, and J. D. Elms, 1993: Comprehensive Ocean–Atmosphere Data Set (COADS) release 1a: 1980–92. *Earth Syst. Monit.*, **4**, 4–8.
- , H. F. Diaz, J. D. Elms, and S. J. Worley, 1998: COADS release 2 data and metadata enhancements for improvements of marine surface flux fields. *Phys. Chem. Earth*, **23**, 517–526.

- Worley, S. J., S. D. Woodruff, R. W. Reynolds, S. J. Lubker, and N. Lott, 2005: ICOADS release 2.1 data and products. *Int. J. Climatol.*, **25**, 823–842.
- Wright, P. B., 1988: An atlas based on the COADS data set: Fields of mean wind, cloudiness and humidity at the surface of the global ocean. Rep. 14 Max-Planck-Institut für Meteorologie, 73 pp.
- Wunsch, C., and P. Heimbach, 2007: Practical global ocean state estimation. *Physica D*, **230**, 197–208, doi:10.1016/j.physd.2006.09.040.
- Yu, J. Y., and C. R. Mechoso, 1999: Links between annual variations of Peruvian stratocumulus clouds and of SST in the eastern equatorial Pacific. *J. Climate*, **12**, 3305–3318.
- Yu, L., X. Jin, and R. Weller, 2008: Multidecade global flux datasets from the objectively analyzed air–sea fluxes (OAFlux) project: Latent and sensible heat fluxes, ocean evaporation, and related surface meteorological variables. Tech. Rep. OA-2008-01, Woods Hole Oceanographic Institution, 64 pp.
- Yu, R., M. Zhang, and R. D. Cess, 1999: Analysis of the atmospheric energy budget: A consistency study of available data sets. *J. Geophys. Res.*, **104**, 9655–9661.
- Zhang, X., W. Lin, and M. Zhang, 2007: Toward understanding the double intertropical convergence zone pathology in coupled ocean–atmosphere general circulation models. *J. Geophys. Res.*, **112**, D12102, doi:10.1029/2006JD007878.
- Zhang, Y., W. B. Rossow, A. A. Lacis, V. Oinas, and M. I. Mishchenko, 2004: Calculation of radiative fluxes from the surface to top of atmosphere based on ISCCP and other global data sets: Refinements of the radiative transfer model and the input data. *J. Geophys. Res.*, **109**, D19105, doi:10.1029/2003JD004457.